Probing Structural and Electronic Properties of the Oxidized $[Fe_4S_4]^{3+}$ Cluster of *Ectothiorhodospira halophila* iso-II High-Potential Iron−Sulfur Protein by ENDOR Spectroscopy

Reinhard Kappl,[†] Stefano Ciurli,[‡] Claudio Luchinat,[§] and Jürgen Hüttermann*,[†]

Contribution from the Institut für Biophysik und Physikalische Grundlagen der Medizin, Uniklinikum Homburg, Universität des Saarlandes, D-66421 Homburg/Saar, Germany, Institute of Agricultural Chemistry, University of Bologna, Viale Berti Pichat 10, I-40127 Bologna, Italy, and Department of Soil Sciences and Plant Nutrition, University of Florence, Piazzale Cascine 28, I-50144 Florence, Italy

Received February 9, 1998. Revised Manuscript Received December 16, 1998

Abstract: The ENDOR response of ^{57}Fe nuclei and protons of the high-potential iron−sulfur (HiPIP) protein iso-II from *Ectothiorhodospira halophila* in frozen solutions, i.e., on nonoriented systems, has been exploited to determine electronic and structural details of the oxidized $[Fe_4S_4]^{3+}$ cluster and its protein environment. Two distinct ^{57}Fe hyperfine couplings were resolved and assigned to pairs of highly symmetric ferric and mixed-valence iron ions in agreement with results of Mössbauer and ENDOR studies on related proteins and model compounds. From the analysis of dipolar contributions of the eight cysteine β-CH_2− and five additional protons of residues close to the cluster, the spin population on the iron ions in the ferric and the mixed-valence pair was deduced. The symmetric spin vector coupling model yields coefficients, which suggest the existence of a $|^7/_2,3,^1/_2\rangle$ state or an admixture of $|^9/_2,4,^1/_2\rangle$ and $|^7/_2,4,^1/_2\rangle$ as possible ground states of the cluster. The identification of the mixed-valence and ferric irons within the cluster was in agreement with NMR results based on the sequence specific assignments of proton couplings. In addition, a unique orientation of the *g*-tensor with respect to the molecular frame was found in the protein, the maximal *g*-tensor component being nearly perpendicular to the cluster face containing the mixed-valence irons. The intermediate and minimal components were related to the vectors connecting the ferric and mixed-valence irons, respectively. The analysis of the isotropic parts of the cysteine β-CH_2-proton interactions allowed establishment of a correlation with the NMR shifts of corresponding protons, obtained by applying different scaling factors for protons close to the ferric and mixed-valence pair, respectively. The empirical law used to describe the relationship between the geometric orientation of a CH bond and the observed isotropic interaction for these types of clusters could be verified.

Introduction

The understanding of the electronic structure of $[Fe_4S_4]^{3+}$ clusters in proteins and models has progressed considerably in recent years.[1−8] These clusters formally contain three ferric ions and one ferrous ion[9] and are characterized by an overall antiferromagnetic Heisenberg coupling, yielding an $S = {}^1/_2$ ground state.[10−12] Vibronic coupling in symmetrical models,[13] intrinsic asymmetry in proteins,[14] and spin frustration in both symmetric and asymmetric compounds[14] concur in the stabilization of a ground state that can be qualitatively described by a ferric−ferric pair antiferromagnetically coupled to a high-multiplicity, mixed-valence ferric−ferrous pair. Due to spin frustration[15] and to the onset of double exchange coupling in the mixed-valence pair,[16,17] the latter has a subspin value exceeding that of the former by $^1/_2$, as was first shown by Mössbauer spectroscopy.[18]

In symmetrical models, the ground state is 6-fold degenerate because the mixed-valence pair can settle on any of the six equivalent iron−iron pairs. Crystal packing forces are apparently sufficient to lift the degeneracy, and at low temperature, the mixed-valence pair is preferentially trapped in only some of

[†] Universität des Saarlandes.
[‡] University of Bologna.
[§] University of Florence.
* Address correspondence to this author at Institut für Biophysik und Physikalische Grundlagen der Medizin, FR 3.6, Uniklinikum, Geb. 76, D-66421 Homburg, FRG.

(1) Beinert, H. *FASEB J.* **1990**, *4*, 2483.
(2) Cammack, R. *Advances in Inorganic Chemistry*, Vol 38; Academic Press: San Diego, CA, 1992; pp 281−322.
(3) Beinert, H.; Holm, R. H.; Münck, E. *Science* **1997**, *227*, 653.
(4) Noodleman, L.; Case, D. A. *Adv. Inorg. Chem.* **1992,** *38*, 424.
(5) Mouesca, J. M.; Chen, J. L.; Noodleman, L.; Bashford, D.; Case, D. A. *J. Am. Chem. Soc.* **1994**, *116*, 11898.
(6) Noodleman, L.; Case, D. A.; Mouesca, J.-M.; Lamotte, B. *J. Biol. Inorg. Chem.* **1996**, *1*, 177.
(7) Blondin, G.; Girerd, J.-J. *J. Biol. Inorg. Chem.* **1996,** *1*, 170.
(8) Banci, L.; Bertini, I.; Ciurli, S.; Ferretti, S.; Luchinat, C.; Piccioli, M. *Biochemistry* **1993**, *32*, 9387.
(9) Carter, C. W. Jr.; Kraut, J.; Freer, S. T.; Alden, R. A.; Sieker, L. C.; Adman, E.; Jensen L. H. *Proc. Natl. Acad. Sci. U.S.A.* **1972**, *69*, 3526.
(10) Beinert, H. *Biochem. Soc. Trans.* **1985,** *13*, 542.
(11) Antanaitis, B. C.; Moss, T. H. *Biochim. Biophys. Acta* **1975**, *405*, 262.
(12) Peisach, J.; Orme-Johnson, N. R.; Mims, W. B.; Orme-Johnson, W. H. *J. Biol. Chem.* **1977**, *252*, 5643.
(13) Bominaar, E. L.; Borshch, S. A.; Girerd, J.-J *J. Am. Chem. Soc.* **1994**, *116*, 5362.
(14) Bertini, I.; Ciurli, S.; Luchinat, C. *Struct. Bonding* **1995,** *83*, 1−53.
(15) Banci, L.; Bertini, I.; Briganti, F.; Luchinat, C.; Scozzafava, A.; Vicens-Oliver, M. *Inorg. Chem.* **1991**, *30*, 4517.
(16) Noodleman, L. *Inorg. Chem.* **1988**, *27*, 3677.
(17) Blondin, G.; Girerd, J.-J. *Chem. Rev.* **1990**, *90*, 1359.
(18) Middleton, P.; Dickinson, D. P. E.; Johnson, C. E.; Rush, J. D. *Eur. J. Biochem.* **1980**, *104*, 289.

10.1021/ja980442z CCC: $18.00
Published on Web 02/17/1999

the six possible positions. This has been demonstrated by EPR and ^{57}Fe and ^{1}H ENDOR studies of model compounds.[19−23]

In proteins, the intrinsic asymmetry is much larger than that induced by crystal packing forces in otherwise symmetric compounds. Therefore, the preference for one of the six possible positions is expected to be stronger. Unfortunately, the resolution of low-temperature Mössbauer data,[18,24] while clearly showing the pairwise arrangement of the iron ions, is insufficient to show that more than one pairwise arrangement is present. Surprisingly, clear evidence for the existence of preferred mixed-valence pair localizations came from room-temperature ^{1}H NMR experiments. The hyperfine-shifted resonances of the β-CH_2 protons of the cluster-coordinated cysteines have been sequence-specifically assigned in a number of $[Fe_4S_4]^{3+}$-containing high-potential iron−sulfur proteins (HiPIP) and interpreted in terms of a preference for two out of the six possible mixed-valence pairs.[8,14,25−28] Interestingly, these two preferential mixed-valence pairs localizations are conserved over the whole class of HiPIPs, the differences among the members of the class being restricted to different populations of the two states. This phenomenon has been termed "electronic isomerism":[29] within a given HiPIP, fast equilibrium is present between the two electronic isomers.[8] The energetic preference for these two isomers over the others must be on the order of kT at room temperature. The picture for proteins, at variance with models, is clearer at room temperature than it is at low temperature, due to the limited resolution of Mössbauer spectroscopy. Indeed, the temperature dependence of the equilibrium constant between the two isomers prevailing at room temperature is not known. EPR spectroscopy at low temperature has given heterogeneous signals for several HiPIPs possibly representing different forms of the isomers.[8,11,24,30,31]

A link between high- and low-temperature electronic structures of HiPIPs could be in principle established by ^{1}H ENDOR spectroscopy, provided the full proton hyperfine tensor can be obtained within the g-tensor frame by measuring the orientation dependence of the ENDOR features.[32−35] Unfortunately, single crystals of proteins suitable for ENDOR spectroscopy are seldom available. Powder-like ENDOR spectra such as those obtained from frozen protein solutions do contain in principle all the necessary information, but its extraction is much more difficult than in the case of single-crystal ENDOR. So far only in the case of the mononuclear centers such as copper(II) in superoxide dismutase[36,37] and for the heme proteins myoglobin and hemoglobin[34,38] could the proton hyperfine tensors be reconstructed using powder-type ENDOR spectra simulations.

In applying this approach to iron sulfur proteins we have chosen the HiPIP iso-II from *E. halophila* since the room-temperature equilibrium between the two electronic isomers for this protein is most shifted to one extreme, making the second isomer undetectable.[27,28] Most importantly, and possibly related to the essence of the problem, this oxidized HiPIP displays an EPR spectrum devoid of any detectable heterogeneity.[24] The aim of the present study, besides that of showing that the approach can be successful, is to compare the electronic structure of the oxidized $[Fe_4S_4]^{3+}$ cluster at low temperature with the picture emerging from high-temperature ^{1}H NMR data. In particular, we want to check whether a single orientation of the mixed-valence pair exists at low temperatures, as found from room-temperature NMR data on this particular protein,[14,27] and, if so, analyze whether the two methods coincide in terms of the orientation. Moreover, a comparison of the directions of the g-tensor axes with respect to the mixed-valence pair in the protein with those obtained from the model compounds is of interest.[21] Finally we want to separate the isotropic (contact plus pseudocontact) contribution to the hyperfine tensor of individual cysteine β-CH_2 protons and compare it with that obtained from room-temperature NMR. Such a comparison should yield information on the ground-state electronic structure, the energy separation of the first excited states, and the adequacy of the current spin coupling models[14,16,17,39−41] for $[Fe_4S_4]^{3+}$ clusters.

Materials and Methods

Preparation of the Protein Samples. Oxidized *E. halophila* iso-II HiPIP (**1**) was isolated and purified according to a previously described procedure.[27] ^{57}Fe-enriched **1** was prepared with the same protocol as above, following growth of the bacteria in ^{57}Fe-enriched medium.[24] All protein samples were kept in 30 mM phosphate buffer, pH 7.2.

The EPR samples of **1** were optimized in concentration (ca. 1 mM) to minimize ENDOR accumulation time. A sample of **1** in deuterated buffer was also prepared using five cycles of solvent exchange with an ultrafiltration Amicon cell equipped with a YM1 membrane, to exchange all solvent-exposed N- or O-bound protons.

EPR and ENDOR Spectroscopy. EPR spectra at X-band frequencies were recorded on Bruker ER 420 or ESP 300 spectrometers equipped with a continuous helium flow cryostat (ESR 900) in a temperature range from 4 to 60 K. The magnetic field and the microwave frequency were determined with a NMR gaussmeter and a microwave counter, respectively. The modulation amplitude for spectra recording was 0.1 mT. Microwave power and temperature were adjusted to obtain optimal signal intensity avoiding spectral broadening.

The ENDOR setup consisted either of a commercial Bruker ENDOR cavity (ER 200 ENB) with a helical rf coil, or a dual cavity with a homemade Helmholtz coil.[42] The rf was generated by a Wavetek Model 3000 synthesizer and amplified with an ENI A150 power amplifier. The rf was frequency modulated with 10 kHz so that ENDOR spectra were recorded as first derivatives. ENDOR measurements were performed between 10 and 20 K. Up to 13 ENDOR spectra were obtained at different working points across the EPR powder spectrum spanning a magnetic field range of ca. 20 mT. The ENDOR spectra

(19) Gloux, J.; Gloux, P.; Lamotte, B.; Rius, G. *Phys. Rev. Lett.* **1985**, *54*, 599.
(20) Gloux, J.; Gloux, P.; Hendriks, H.; Rius, G. *J. Am. Chem. Soc.* **1987**, *109*, 3220.
(21) Gloux, J.; Gloux, P.; Lamotte, B.; Mouesca, J.-M.; Rius, G. *J. Am. Chem. Soc.* **1994**, *116*, 1953.
(22) Rius, G.; Lamotte, B. *J. Am. Chem. Soc.* **1989**, *111*, 2464.
(23) Mouesca, J.-M.; Rius, G.; Lamotte, B. *J. Am. Chem. Soc.* **1993**, *115*, 4714.
(24) Bertini, I.; Campos, A. P.; Luchinat, C.; Teixeira, M. *J. Inorg. Biochem.* **1993**, *52*, 227.
(25) Banci, L.; Bertini, I.; Briganti, F.; Scozzafava, A.; Vicens-Oliver, M.; Luchinat, C. *Inorg. Chim. Acta* **1991**, *180*, 171.
(26) Bertini, I.; Briganti, F.; Luchinat, C.; Scozzafava, A.; Sola, M. *J. Am. Chem. Soc.* **1991**, *113*, 1237.
(27) Banci, L.; Bertini, I.; Capozzi, F.; Carloni, P.; Ciurli, S.; Luchinat, C.; Piccioli, M. *J. Am. Chem. Soc.* **1993**, *115*, 3431.
(28) Bertini, I.; Ciurli, S.; Dikiy, A.; Luchinat, C. *J. Am. Chem. Soc.* **1993**, *115*, 12020.
(29) Bertini, I.; Luchinat, C. *Transition metal sulfur chemistry*; ACS Symposium Series 653; American Chemical Society: Washington, DC, 1996; pp 57−73.
(30) Dunham, W. R.; Hagen, W. R.; Fee, J. A.; Sands, R. H.; Dunbar, J. B.; Humblet, C. *Biochim. Biophys. Acta* **1991**, *1079*, 253.
(31) Beinert, H.; Thomson, A. J. *Arch. Biochem. Biophys.* **1983**, *222*, 333.
(32) Rist, G.; Hyde, J. S. *J. Chem. Phys.* **1969**, *52*, 4633.
(33) Schweiger, A. *Struct. Bonding* **1982**, *51*, 1−122.
(34) Kappl, R.; Hüttermann, J. *Advanced EPR*; Elsevier: Amsterdam, 1989; pp 501−540.
(35) Hoffman, B. M.; Gurbiel, R. J.; Werst, M. M.; Sivaraja, M. J. *Advanced EPR*; Elsevier: Amsterdam, 1989; pp 541−592.
(36) Hüttermann, J., Kappl, R.; Banci, L.; Bertini, I. *Biochim. Biophys. Acta* **1988**, *956*, 173.
(37) Reinhard, H.; Kappl, R.; Hüttermann, J.; Viezzoli, M.-S. *J. Phys. Chem.* **1994**, *98*, 8806.
(38) Hüttermann, J.; Burgard, C.; Kappl, R. *J. Chem. Soc., Faraday Trans.* **1994**, *90*, 3077.

extended over a frequency range from 1 to 36 MHz. The spectral accumulation time varied between 40 and 2000 s.

Simulation of ENDOR Powder Spectra. The program Prometheus was employed for simulation of powder ^{1}H-ENDOR spectra. This program allows to interactively fit the simulated resonance pattern to an experimental one. It is based on the formalism described by Kreilick et al.,[43,44] which uses the point dipole approximation for calculation of the dipolar hyperfine interaction of a proton for an orientation selection determined by the working point within the EPR spectrum (i.e., the magnetic field or the effective *g*-factor). A similar method has been developed by Hoffman and co-workers.[45,46] The program, which has been described in detail recently,[47] is designed to be applicable to systems with rhombic *g*-symmetry and arbitrary arrangement of metal (and/or ligand) hyperfine tensors. In particular, when a given hyperfine tensor is collinear with the *g*-tensor, then the orientation selection is calculated by an analytical expression. This avoids artifacts in the simulated pattern arising from an insufficient number of randomly generated orientations and reduces processing time considerably.[47] The program uses as input a spatial structure (Brookhaven Protein Databank pdb-format) of the active site of a protein or a putative related structure from which atoms with electron spin density (up to 10) and interacting protons (up to 20) can be selected. The individual spin populations, optional isotropic interactions for protons, the arrangement of the *g*-tensor with respect to the molecular frame as well as the spatial positions of the protons can be varied. The interaction of a proton with each spin center is calculated componentwise and summed up for all the selected *g*-orientations determined by the ENDOR working point within the separately simulated EPR spectrum. The shape of a powder spectrum for a single proton is obtained by folding the calculated resonance positions with a mathematical line shape function (i.e., first derivative of a Gaussian in our case). The final simulated powder spectrum is then composed of ENDOR spectra of all selected protons.

Small variations of the position of an interacting proton within the ensemble of molecules which provoke a distribution of resonance frequencies and thus line broadening in the experimental spectrum pose a problem when comparing with simulations. The effect is more pronounced for protons close to spin centers due to the r^{-3} dependence of the dipolar interaction as was described in a protein single-crystal ENDOR study.[48] Also the intrinsic variability of magnetic parameters (*g*-strain, *A*-strain) within the ensemble of molecules contributes significantly to EPR as well as ENDOR powder line shapes.[49] Superposition of successively simulated ENDOR spectra with slightly different parameters (*g*-tensor values or directions, A_{iso}) can be used to mimic such a variability. In this study, the effect of *g*-strain could be analyzed for a single proton.

A simulated powder-type pattern for all contributing protons represents a compromise with respect to the mentioned parameters and may not completely reproduce all the experimental details of a powder ENDOR spectrum. For an analysis of the behavior of an individual proton across the EPR powder spectrum a field-frequency plot is helpful. In this, the experimental resonance positions, normalized to the free proton frequency with $\nu_H = 0$ are plotted for all experimental fields. The data points represent the line maxima or the points of steepest slope for monophasic (above or below the baseline) and biphasic (above and below the baseline) line shapes, respectively, but the line width is not included. In this representation the experimental frequencies can be compared with simulated ones (usually of the extremal turning points) for the same field positions (or *g*-factors). In such a way the arrangement of a *g*-tensor orientation within the molecular frame can be tested, to which particularly the behavior of dipolar couplings is sensitively responding. To determine the isotropic contributions of the cysteine β-CH_2 protons, the line behavior of each proton for several isotropic values was examined in the field-frequency plot. The best combinations were selected and used again for simultaneous simulations of all interacting protons.

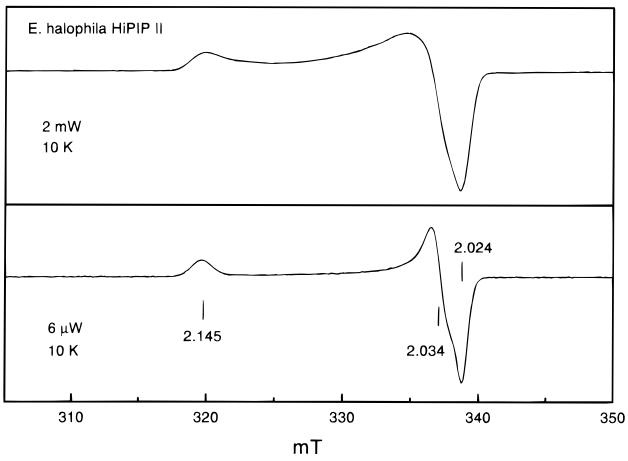

Figure 1. EPR spectra of **1** (X-band, 9.5 GHz, at 10 K, modulation amplitude 0.1 mT) obtained for microwave powers of 2 mW (top) and 6 μW (bottom). At high powers the spectrum broadens considerably. The *g*-tensor values used for simulation are indicated in the lower trace. No additional peaks associated with further spectral species are apparent.

Results

EPR Spectroscopy. The EPR spectrum of **1** shows the typical features of oxidized HiPIPs, generally observable in EPR only below liquid nitrogen temperatures, exhibiting average *g*-factors $g_{av} > 2$. The spectrum of Figure 1, recorded under nonsaturating conditions (6 μW, bottom trace), shows a pattern of slight rhombic distortion with principal *g*-tensor components $g = 2.145$, 2.034, and 2.024 determined from simulation. When higher microwave powers (2 mW, top trace) or lower temperatures are applied, the spectral shape is broadened until the rhombic feature eventually disappears. In agreement with previous data,[24] and in contrast to the EPR spectra of other HiPIPs isolated from *C. vinosum*, *E. vacuolata* iso-I and iso-II, *R. gelatinosus*, *C. tepidum*, and *Rf. fermentans*,[14,30,50,51] no additional weak resonances associated with the presence of minor species and/or with dimer formation[11,30,31] are observed, so that the spectrum of **1** is considered to arise from a single species.

In samples substituted with ^{57}Fe, the line width is not significantly broadened. As a consequence, the hyperfine interaction of the unpaired electron with the ^{57}Fe nuclei ($I = {}^1/_2$) remains inaccessible to EPR spectroscopy.

^{57}Fe-ENDOR. The ENDOR spectra for three representative *g*-factors obtained on the ^{57}Fe-substituted sample in the frequency range 9−20 MHz are depicted in Figure 2. Apart from

(39) Mouesca, J.-M.; Noodleman, L.; Case, D. A.; Lamotte, B. *Inorg. Chem.* **1995**, *34*, 4347.
(40) Belinskii, M.. I.; Bertini, I.; Galas, O.; Luchinat, C. *Z. Naturforsch.* **1995**, *50a*, 75.
(41) Belinskii, M. I.; Bertini, I.; Galas, O.; Luchinat, C. *Inorg. Chim. Acta* **1996**, *243*, 91.
(42) Hüttermann, J.; Kappl, R. *Metal Ions in Biological Systems*; Marcel Dekker: Basel, 1987; Vol. 22, pp 1−80.
(43) Hurst, G. C.; Henderson, T. A.; Kreilick, R. W. *J. Am. Chem. Soc.* **1985**, *107*, 7294.
(44) Henderson, T. A.; Hurst, G. C.; Kreilick, R. W. *J. Am. Chem. Soc.* **1985**, *107*, 7299.
(45) Hoffman, B. M.; Martinsen, J.; Venters, R. A. *J. Magn. Res.* **1984**, *59*, 110.
(46) Hoffman, B. M.; Venters, R. A.; Martinsen, J. *J. Magn. Res.* **1985**, *62*, 537.
(47) Hüttermann, J.; Däges, G. P.; Reinhard, H.; Schmidt, G. *Nuclear Magnetic Resonance of Paramagnetic Macromolecules*; Kluwer Academic Publishers: Dordrecht, The Netherlands, 1995; pp 165−192.
(48) Kappl, R.; Hüttermann, J. *Isr. J. Chem.* **1989**, *29*, 73.
(49) Neese, F.; Kappl, R.; Hüttermann, J.; Zumft, W. G.; Kroneck, P. M. H. *J. Biol. Inorg. Chem.* **1998,** *3*, 53.
(50) Moulis, J.-M.; Scherrer, N.; Gagnon, J.; Forest, E.; Petillot, Y.; Garcia, D. *Arch. Biochem. Biophys.* **1993**, *305*, 186.
(51) Hochkoeppler, A.; Kofod, P.; Ferro, F.; Ciurli, S. *Arch. Biochem. Biophys.* **1995**. *322*, 313.

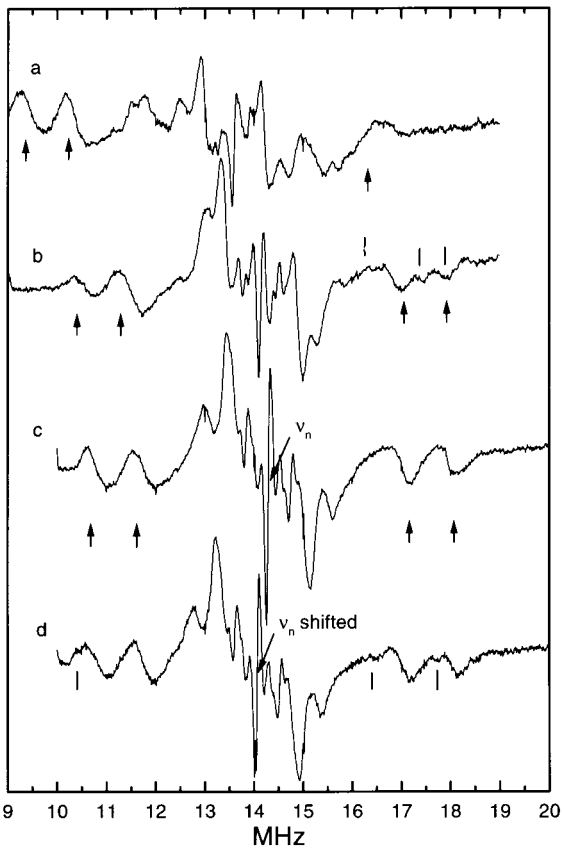

Figure 2. ENDOR spectra of ^{57}Fe-substituted **1** at three *g*-selections: (a) $g = 2.143$, (b) $g = 2.053$, and (c, d) $g = 2.030$. Spectrum d was obtained with a frequency-shifted cavity so that for the same *g*-selection as in spectrum c the different magnetic field displaces the free proton frequency and proton lines. The two groups of ^{57}Fe resonances are marked with arrows, and the superimposed ^{1}H resonances are indicated by sticks.

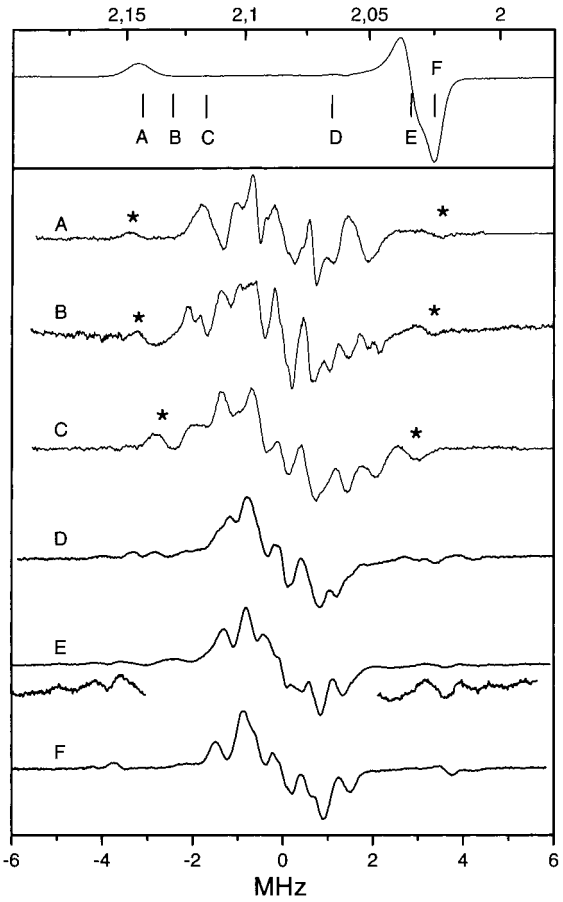

Figure 3. ENDOR spectra of **1** (^{56}Fe in natural abundance) at selected *g*-factors indicated by letters in the EPR spectrum (top, scale of the EPR is the *g*-factor). The ENDOR spectra are normalized to the corresponding free proton frequency to illustrate the evolution of lines across the EPR spectrum for various field positions. The asterisks mark the lines arising from Phe44 Hβ1-proton (HCB) in the region of g_1 before they merge with other proton resonances.

resonances centered around the free proton frequency ν_n, two relatively intense pairs of signals are discernible on the low- and on the high-frequency side of ν_n (e.g., trace c). One is centered at about 11.5 MHz, the other at about 17.5 MHz. Each line of the pair is separated from the other by about 0.9 MHz which corresponds to the Larmor splitting ($2\nu_{Fe}$) for ^{57}Fe at X-band magnetic fields. These resonances are absent in samples with ^{56}Fe in the cluster (compare Figure 3, trace E at frequencies +2.7, +3.6 MHz and −2.5, −3.5 MHz) so that the lines marked with arrows in Figure 2 are attributed to two Larmor-split ^{57}Fe resonances. A downward shift in microwave frequency by approximately 0.8 GHz reveals some weak lines which move to lower frequencies, concomitantly with the free proton frequency ν_n (Figure 2, trace d), at the same *g*-factor as in trace c, indicating that the lines originate from weakly coupled protons (marked with sticks). The two groups of ^{57}Fe resonances, on the other hand, remain essentially unaltered in their position, since they are centered around $A(^{57}\text{Fe})/2$. Thus, the ^{57}Fe-hyperfine values directly read from the ENDOR spectrum have an error margin of ca. ±0.3 MHz because of the superposition with proton lines and the rather large line width. It is obvious from Figure 2 (trace a) that for this field position ($g = 2.143$) the $A(^{57}\text{Fe})$ values can be determined for the low-frequency signal but have to be estimated for the high-frequency doublet because the latter lines are buried under the rather intense central proton resonances. For other *g*-factors (Figure 2, trace b) the ^{57}Fe resonances emerge from a gamut of lines and appear more clearly. When the field position is changed within the nearly axial part of the EPR spectrum (from $g = 2.040$ to 2.030) the resonance frequencies of both doublets remain nearly identical. The coupling values found for each Larmor-split doublet along the principal *g*-components are compiled in Table 1 for **1** and compared to Mössbauer[24] and ENDOR data on oxidized *C. vinosum* HiPIP (**2**)[18,52] and model compounds.[22,53] The two groups of doublets found in the ^{57}Fe ENDOR spectrum of **1** are assigned to the ferric and mixed-valence pairs of iron ions as detected by Mössbauer spectroscopy.[18,24,53] In principle, for each individual ^{57}Fe ion of the cluster, a Larmor-split doublet is expected. Four groups of doublets have indeed been observed in the well-resolved single-crystal ENDOR spectra of $[Fe_4S_4(SCH_2C_6D_5)_4]^{1-}$ (**3**).[22] A resolution of the individual ^{57}Fe doublet lines within a pair in the powder ENDOR spectra of **1** is prevented by nearly identical hyperfine components (within ±0.3 MHz) and the superposition of slightly different contributions due to a small anisotropy for a given *g*-selection, for which the spectral intensity is distributed over an increased frequency range. These factors could be the source of the larger line widths (0.5−1 MHz) observed for **1** as compared with those of **3** (0.1−0.2 MHz).

^{1}H ENDOR. Some representative ENDOR spectra obtained from a sample of **1** with naturally abundant ^{56}Fe are shown in

(52) Anderson, R. E.; Anger, G.; Petersson, L.; Ehrenberg, A.; Cammack, R.; Hall, D. O.; Mullinger, R., Rao, K. K. *Biochim. Biophys. Acta* **1975**, *376*, 63.

(53) Papaefthymiou, V.; Millar, M. M.; Münck, E. *Inorg. Chem.* **1986,** *25*, 3010.

Table 1. ^{57}Fe Couplings for $[Fe_4S_4]^{3+}$ Clusters in Proteins and Model Compounds

	oxidized *E. halophila* iso-II HiPIP (**1**)		
powder ENDOR along *g*-factor	group I *A* (MHz) ± 0.3	group II[a] *A* (MHz) ± 0.3	this work
2.140	19.8	<32	
2.030	22.4	35	
2.020	22.2	35.1	
average	21.6	33	
	oxidized *E. halophila* iso-II HiPIP (**1**)		
Mössbauer (in MHz)	ferric pair ±1.5	mixed-valence pair ±1	ref 24
A_{xx}	21.9	−29.5	
A_{yy}	21.9	−32.1	
A_{zz}	20.3	−32.9	
average	21.4	−31.5	
powder ENDOR (in MHz)	oxidized *C. vinosum* HiPIP (**2**)		
	group I	group II	ref 52
$A_{\|\|}$	21.2 ± 0.1	29.8 ± 0.8	
$A_{\perp}$	22.8 ± 0.1	32.0 ± 0.2	
average	22	30.9	
Mössbauer (in MHz)	oxidized *C. vinosum* HiPIP (**2**)		
	ferric pair	mixed-valence pair	ref 18
A_{xx}	19.2 ± 1.3	−28.2 ± 1.9	
A_{yy}	22.4 ± 0.8	−30.6 ± 0.6	
A_{zz}	19.3 ± 0.8	−32.6 ± 0.8	
average	20.3	−30.5	
single-crystal ENDOR (in MHz)	$[Fe_4S_4(SCH2C_6D_5)_4]^{1-}$ (**3**)		
	ferric pair	mixed-valence pair	ref 22
A_{min}	18	−30.1	
A_{int}	19.6	−33.9	
A_{max}	21.8	−36.5	
average	19.8	−33.5	
Mössbauer (in MHz)	$[Fe_4S_4(S\text{-}2,4,6\text{-}i\text{-}Pr_3C_6H_2)_4]^{1-}$ (**4**)		
	ferric pair	mixed-valence pair	ref 53
A_{xx}	21.9	−28.1	
A_{yy}	20.6	−32.2	
A_{zz}	18.5	−32.9	
average	20.3	−31.1	

[a] The sign could not be directly determined, but the values should be associated with a negative sign from comparison with the other data.

Figure 3. The corresponding working points are indicated as letter code in the EPR spectrum (insert). For all ENDOR spectra the free proton frequency associated with each working point was set to zero in order to emphasize the evolution of lines depending on the selected field (or *g*-factor). The large signal intensity around the free proton frequency (±1 MHz) is mainly due to many weakly coupled protons at distances larger than 4.5 Å from the cluster, while the larger couplings are originating from fewer protons close to the cluster. The line pattern generally is rather symmetrical around ν_n with line width between 0.4 and 1 MHz for the outer lines. Such ENDOR line widths are often found in proteins in which structural disorder at low temperatures leads to a distribution of relevant magnetic parameters (*g*-strain, *A*-strain).[34,48]

A frequency range from 1 to 36 MHz was scanned in order to detect possible ^{14}N interaction or very large proton couplings (then centered around *A*/2). However, no indications for such interactions were found. The largest proton hyperfine splitting of ca. 10 MHz is observed around $g = 2.034$, as shown in trace E of Figure 3 with enhanced outermost lines. Along $g = 2.145$ (Figure 3, trace A) a well-separated extreme line pair is visible (marked by asterisks) with a splitting of 6.8 MHz which decreases in traces B and C. Exchange of the aqueous buffer with D_2O, which has often proven helpful in quantifying exchangeable NH or OH protons in the cluster neighborhood (e.g., refs 54−56), has not been successful in the present case. Only subtle if any changes of line intensities were observed in the range of ±1.5 MHz, with no clear loss of resonances (data not shown). The larger couplings remained completely unaffected, indicating that they arise from nonexchangeable protons.

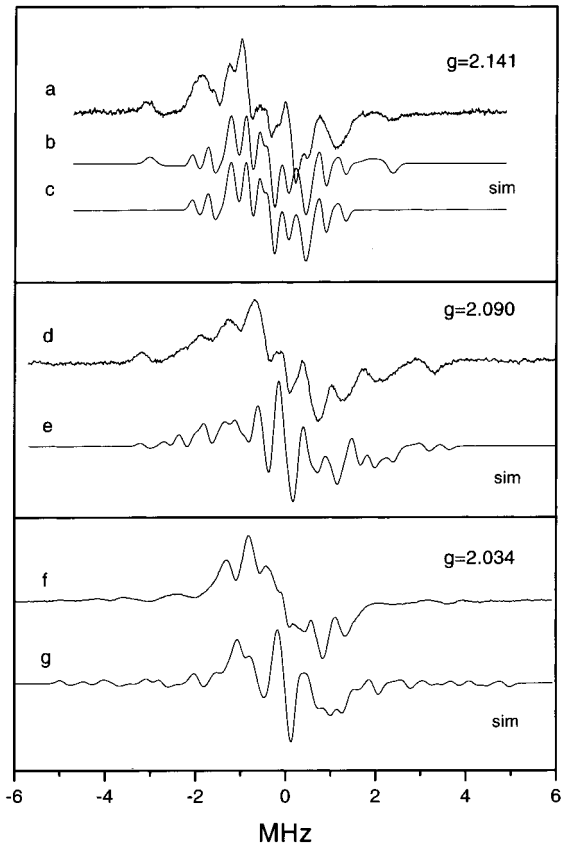

Figure 4. Comparison of experimental ENDOR spectra for some representative *g*-selections [(a) $g = 2.141$, (d) $g = 2.090$, and (f) $g = 2.034$] to related simulated patterns (b, c, e, g) with all protons of Chart 2 included. In simulation c the interaction of the Hβ1 proton of Phe44 is switched off to notify the assignment of the extreme resonances to this proton.

To visualize the variation of ENDOR lines across the EPR spectrum, the line positions for all working points with ν_n set to zero were plotted versus the magnetic field scale (field-frequency plot) in Figure 5A, which shows the gradual decrease of the outermost line pair in the region of g_1, followed by an increase to the maximal splitting along g_2.

Simulation of ^{1}H-ENDOR Spectra. There is no X-ray determined crystal structure information on HiPIP iso-II available. The starting point for the ENDOR simulations was therefore the structural model of **1**[27] which was obtained by molecular dynamics calculations on the sequence adjusted X-ray structure of isoenzyme I of *E. halophila*.[57] The cluster atoms and the four ligating cysteines 39, 42, 55, and 71 (up to Cα

(54) Werst, M. M.; Kennedy, M.-C.; Beinert, H.; Hoffman, B. M. *Biochemistry* **1990**, *29*, 10526.
(55) Doan, P. E.; Fan, C.; Hoffman, B. M. *J. Am. Chem. Soc.* **1994**, *116*, 1033
(56) Hoffman, B. M.; DeRose, V. J., Doan, P. E., Gurbiel, R. J., Houseman, A. L. P.; Telser, J. In *Biological Magnetic Resonance*; Berliner, L. J., Reuben, J., Eds.; Plenum Press: New York, 1993; pp 151−218

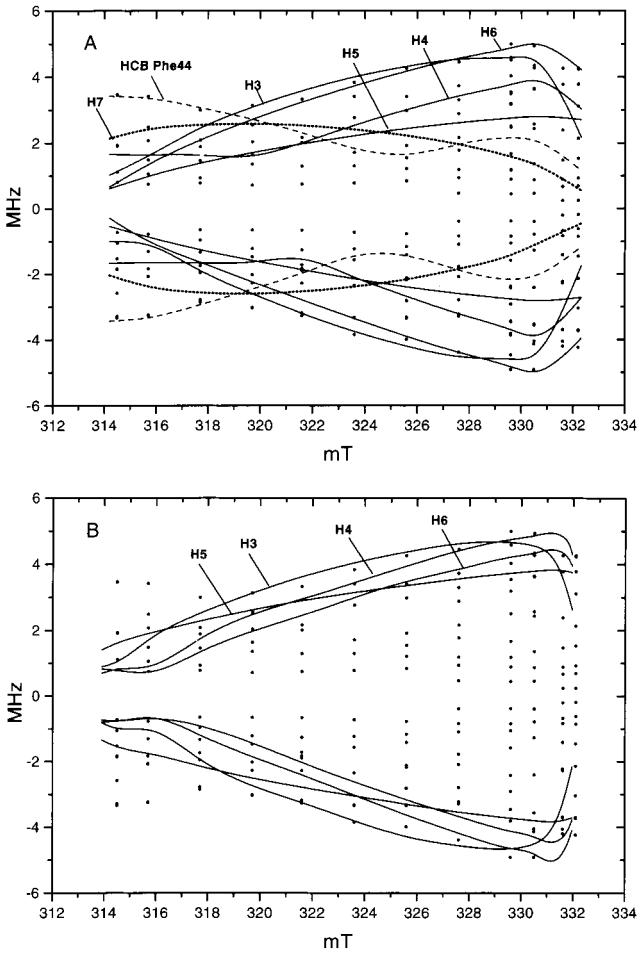

Figure 5. (A) Representation of ENDOR resonances at all experimental field positions on the EPR spectrum (field-frequency plot). The data points correspond to the maxima of monophasic or to steepest slope of biphasic lines and are normalized to the free proton frequency for each field. Experimental line widths are omitted for the sake of clarity. The extremal resonances obtained from simulations of individual protons for all fields are projected onto experimental data points. The variations for HCB Phe44 (dashed line), for cysteine β-CH_2 protons H3 to H6 (isotropic values of set I, Table 2) close to the mixed-valence irons (solid line) and for cysteine β-proton H7 (dotted line) close to a ferric iron are indicated. (B) Projection of extremal resonances simulated for cysteine β-protons H3 to H6 (isotropic values of set II, Table 2) close to the mixed-valence irons. For assignment of protons refer to Charts 1 and 2.

atoms) taken from the MD structure are depicted and specified in Chart 1. The largest spheres mark the iron atoms, the medium-sized dark-gray spheres represent the inorganic and cysteine sulfur atoms, and the small light-gray spheres are the cysteine β-CH_2 protons which are at distances between 3.2 and 3.9 Å to the iron ion to which the cysteine is bound. The arrangement of the four cysteine arms with respect to the cluster is only slightly altered when compared to the crystal structure of *E. halophila* iso-I HiPIP.[57]

The next prerequisite for the simulation is to choose those iron atoms constituting the mixed-valence pair, i.e., having positive spin populations, while the other pair consequently is ferric, with negative spin populations. As outlined above, there are, in principle, six possibilities for the assignment of the two pairs. However, in a recent NMR study on oxidized **1**,[27] the paramagnetic shifted ^{1}H NMR resonances of all eight cysteine β-CH_2 protons were identified by sequence specific assignment. It was demonstrated that four downfield shifted ^{1}H NMR lines arise from β-CH_2 protons of Cys42 and Cys55, which therefore have to be bound to the mixed-valence pair. Conversely, the four upfield shifted signals were assigned to β-CH_2 protons of Cys39 and Cys71, bound to the ferric irons of the cluster. According to this assignment, Fe2 and Fe3 in Chart 1 were chosen as the mixed-valence pair (large dark-gray spheres) and Fe1 and Fe4 as the ferric pair (large open spheres).

As a further parameter the orientation of the *g*-tensor must be fixed. On the basis of both single-crystal EPR data of **3**[21,22] and of theoretical considerations,[58] it can be assumed that (i) the minimal *g*-factor g_3 is closely correlated to the vector connecting the iron ions of the mixed-valence pair, (ii) the intermediate *g*-factor g_2 is correlated to the vector connecting the iron ions of the ferric pair, and (iii) the maximal *g*-factor g_1 is nearly perpendicular to the two cluster faces containing the mixed-valence pair Fe2−Fe3 and the ferric pair Fe1−Fe4. Finally, from the similarity of the ^{57}Fe-hyperfine interactions of **1** and **3** (Table 1) and their correlation to spin densities obtained from the analysis of dipolar contributions of proton interactions in **3**,[23] the expected range of the spin populations on the iron atoms is estimated to be within 1.0 and 1.5 for the mixed-valence and within −0.5 and −1.0 for the ferric irons.

With these prerequisites systematic simulations were performed with eight operative spin centers, i.e., the four iron ions and the four cysteinyl sulfur atoms. For the latter, spin populations between −0.10 and 0.10 were tested. Contributions arising from inorganic sulfurs were neglected because of their larger distances to interacting cysteine β-CH_2 protons and their expected low spin densities.[23] The size of the dipolar ("through space") interaction is then determined by the distances between each proton and each spin center and by the *g*-orientation selected by the ENDOR field position. Another variable affecting the ENDOR line positions is the isotropic hyperfine contribution due to the summation of pseudocontact coupling, arising from magnetic susceptibility anisotropy, and of contact coupling, arising from spin density delocalization via the bonds connecting the residue to a spin center. Hence, the isotropic couplings of all eight cysteine β-CH_2 protons were varied independently employing negative or positive contributions for those close to ferric sites or to mixed-valence iron ions, respectively. For each cysteine β-CH_2 proton the line behavior was studied and compared to the experimental pattern for several field positions in the EPR spectrum, resulting in a reduction of possible combinations of spin distribution and isotropic couplings. In a similar way, purely dipolar coupled protons in the vicinity of the cluster were successively included in the simulations. A sketch of the arrangement of relevant and potentially relevant protons around the cubane is given in Chart 2. The cysteine β-CH_2 protons are colored black, and protons of other residues depicted as open circles. Altogether, apart from the eight cysteine β-CH_2 protons, there are nine dipolar protons seen to occur within a sphere of about 4 Å around the spin centers which were tested for their effects on the ENDOR spectra by simulation. Three of them will be discussed below.

The results of the simulation procedure are shown in Figure 4 for three representative field positions. The experimental spectrum at $g = 2.141$ (trace a) is compared with two simulations. Trace b contains all protons considered, whereas in trace c, the purely dipolar coupled Phe44 Hβ1 (HCB) was omitted from simulation. From this comparison it can be

(57) Breiter, D. R.; Meyer, T. E.; Rayment, I.; Holden, H. M. *J. Biol. Chem.* **1991**, *266*, 18660.

(58) Le Pape, L.; Lamotte, B.; Mouesca, J.-M.; Rius, G. *J. Am. Chem. Soc.* **1997**, *119*, 9757.

Chart 1

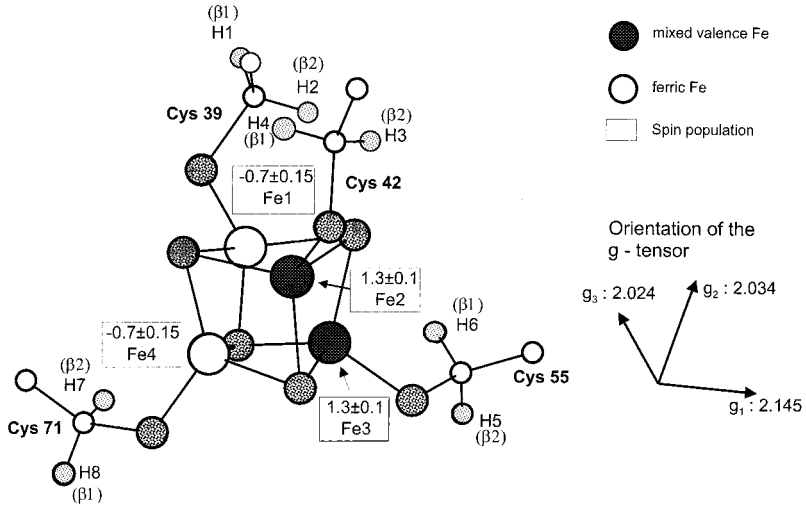

Chart 2

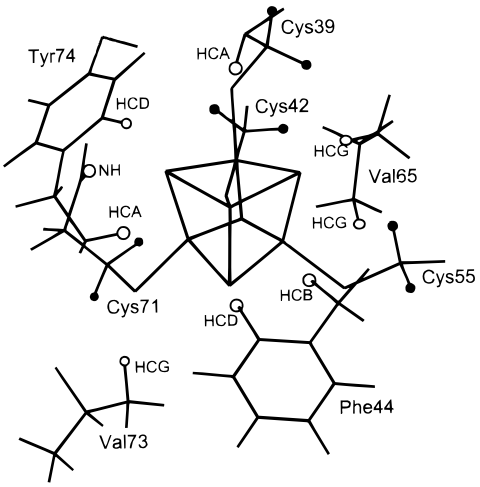

concluded that Phe44 Hβ1 clearly gives rise to the extremal line pair seen in traces a and b, showing a splitting of 6.8 MHz. The large magnitude of this interaction is caused by the rather symmetric position of the proton with respect to the mixed-valence iron ions, for which a high spin population around 1.3 is required in simulations (see Chart 1). For this proton, the simulated line shape models the experimental one very closely after introducing *g*-strain (from 2.1550 to 2.1433, Figure 4, trace b, see also Materials and Methods). The simulated variation of the extremal resonances of this proton for smaller *g*-factors than g_1 is shown in the field-frequency plot of Figure 5A (lines HCB Phe44), which precisely follows the experimental data points before merging with other lines. This characteristic behavior could not be reproduced with any cysteinyl β-CH_2 protons or any other dipolar coupled proton for any alternative configuration of spin centers and *g*-tensor (see below). Thus, this finding confirms the NMR assignment of the mixed-valence pair to Fe2 and Fe3.[27] It also supports the chosen orientation of the maximal *g*-factor perpendicular to this cubane face and the values of the mixed-valence irons' spin populations.

It is noted that along g_1, apart from the interaction of Phe44 Hβ1 proton, no other hyperfine coupling exceeds 4.5 MHz. For other *g*-orientations (Figure 4, traces d−g) the spectral range is spread over ca. 10 MHz. Concomitantly, rather broad and weak outer lines are observed (e.g., trace f) which are mainly due to interactions of cysteine β-CH_2 protons close to the mixed-valence pair. Several proton lines or various values of the isotropic hyperfine coupling can be used to fit such a broad experimental resonance. This possible spectral overlap within broad lines is the main reason for not obtaining one definite value of the isotropic contribution for each cysteine β-CH_2 protons. As a matter of fact, two sets of isotropic contributions for cysteine protons in the vicinity of the mixed-valence irons were extracted, which fit the experimental line behavior over the range of EPR field positions roughly equally well (sets I and II, listed in Table 2).

To visualize the validity of the chosen parameters for all field positions, the variation of the extreme turning points of simulated patterns (i.e., the maximal coupling for a certain *g*-selection) for selected cysteine β-CH_2 protons are projected onto the ENDOR line positions in the field-frequency plot (Figure 5A,B). The resulting curves calculated with isotropic couplings of set I (Table 2) for the four β-CH_2 protons attached to Cys42 and Cys55 (i.e., H3−H6), bound to the mixed-valence iron ions, are shown in Figure 5A. They cover the larger couplings in the region of g_2 and g_3. In particular, Cys42 Hβ2 (H3) and Cys55 Hβ1 (H6) are responsible for the extreme lines, while their vicinal partners Cys42 Hβ1 (H4) and Cys55 Hβ2 (H5) contribute more to the inner features (with couplings of 4 to ca. 7 MHz). The line variations calculated for protons H3, H4, H5, and H6 using the isotropic couplings of set II are shown in Figure 5B. These lines are now more confined to the outer experimental points. It is not possible, only by spectra comparison, to clearly favor either set I or set II of isotropic values, and for the moment, both sets are retained for discussion.

From the group of protons close to the ferric iron ions (Cys39 Hβ1 (H1) and Hβ2 (H2) and Cys71 Hβ1 (H8) and Hβ2 (H7)) spectral contributions are found in a range up to ±3.5 MHz around the free proton frequency. Their extremal couplings are severely overlapping with other spectral components of H3 to H6 and further dipolar protons for most of the field positions. Only for proton H7 a unique contribution to the line variation in the region of g_1 can be obtained, which is also shown in Figure 5A. As a consequence, it is not possible in each case to determine isotropic contributions directly and unambiguously, but estimates can be given (Table 2). These mainly rely on the condition to restrict them to the experimental pattern within ±2 MHz in the g_1-region and to avoid interference with the extremal lines of H3−H6 close to the mixed-valence irons.

A separate analysis of the interactions of purely dipolar protons within 4.0 Å around the cluster (cf. Chart 2) reveals that, apart from Phe44 Hβ1, no maximal coupling value larger than

Table 2. Comparison of Isotropic Hyperfine Couplings of Cysteine β-CH_2 Protons from **1** Derived from Simulation of ENDOR Spectra with Values Calculated from Paramagnetic Shifts of NMR from **1** and with Data from Model Compound **3**

proton (Chart 1)	set I A_{iso} (MHz) ENDOR	set II A_{iso} (MHz) ENDOR	A_{iso} (MHz) ENDOR (calcd from NMR)	^{1}H NMR hyperfine shifts (ppm), ref 27	A_{iso} (MHz) ENDOR (single crystal of **3**), ref 23
H5 (Cys55 Hβ2)	1.8	3.9[a]	3.9	98	3.63 (A6)
H6 (Cys55 Hβ1)	3.3[a]	2.2[a]	2.0	51	1.86 (A5)
H3 (Cys42 Hβ2)	2.0[a]	2.3[a]	2.3	59	2.60 (A8)
H4 (Cys42 Hβ1)	(0.8)	(2.6)	1.9	48	1.60 (A7)
H2 (Cys39 Hβ2)	(−1.8)	(−1.8)	−1.5	−32	−1.80 (A2)
H1 (Cys39 Hβ1)	(−1.6)	(−1.6)	−1.4	−30	−1.95 (A1)
H7 (Cys71 Hβ2)	−1[a]	−1[a]	−1.0	−21	−1.04 (A3)
H8 (Cys71 Hβ1)	(−1.5)	(−1.5)	−1.3	−27	−2.00 (A4)

[a] The marked values show a critical influence on the ENDOR simulations and are determined to ±0.3 MHz. The other couplings (in parentheses) are more variable. Due to the low resolution within broad lines the values cannot be assigned unambiguously. The error margin is estimated with ±1 MHz. The calculated A_{iso} values from paramagnetic shifts were normalized to ENDOR values for H5 and H7, respectively; for details see text. Sets I and II for isotropic couplings could be distinguished only for the mixed-valence bound cysteine β-CH_2 protons. Couplings from model compound **3** (ref 23) were grouped according to the closest agreement with protein data.

ca. 5 MHz is expected for any field position, thus underlining the exceptional behavior of Phe44 Hβ1. The Tyr74 Hα proton, which lies at 3.5 Å from the mixed-valence Fe2, is contributing to the extremely broad line at ±2.5 MHz in the g_2-region (e.g., Figure 3, trace E), but an isolated line cannot be assigned because of overlap with several other resonances and the pronounced powder character. In a similar way, for Cys39 Hα, close to Fe1 (ca. 3.1 Å), the maximal splitting of 4.8 MHz is reached around $g = 2.09$, where there is overlap with an extremely broad line expanding from ±1.7 to ±2.8 MHz (Figure 4, traces d and e). In the ±1.5 MHz frequency range around ν_H, only small if any changes in line intensities are detected in the spectrum of the sample dissolved in D_2O. This observation is in agreement with what is expected. Unlike the case of the reduced $[Fe_4S_4]$ cluster of aconitase[54] and of $[Fe_3S_4]$ in reduced hydrogenase[55] in which the significant hydrogen bonding occurring between cluster iron(s) and ligands could be exploited to yield structural information, only one potentially exchangeable proton (Cys71 NH) is found in the vicinity of an iron ion in the structure of **1**. This proton, close to ferric Fe4, would yield maximal couplings of ca. 3 MHz. Further dipolar protons are mainly contributing to the central parts of the ENDOR spectra, which however are inaccessible to a detailed analysis.

So far, the reasonable agreement between simulation of a large number of interactions and the experiment is obtained with the configuration of magnetic parameters summarized in Chart 1, which is supported by information from NMR and model system ENDOR studies. To verify this configuration several alternatives for the arrangement of *g*-tensor, assignment of the mixed-valence pair and the spin density distribution were tested by analyzing both the dipolar interactions of vicinal protons and the dipolar contribution of the cysteinyl β-CH_2 protons because these contributions are extremely sensitive to the effective distance ($\sim 1/r^3$) from the spin centers and to the angular selection. If, for example, the *g*-tensor is rotated such that g_1 is perpendicular to the face containing Fe1 and Fe2, the largest couplings (again up to ca. 10 MHz) are then obtained in the g_1-region, and the minimal ones along g_2. Thus, the symmetry of the line behavior for this configuration is drastically changed and cannot be adjusted to the experimental behavior (cf. Figures 5A,B) by any reasonable variation of simulation parameters. In addition, further configurations with the mixed-valence pair on Fe2−Fe4 and related *g*-tensor orientation as well as an interchange of g_2 and g_3 directions could be ruled out as alternative possibilities by this procedure, thus validating the configuration suggested in Chart 1.

Finally, some comments apply to the precision and the error margins of the magnetic parameters determined from fits of simulated patterns to the experimental spectra showing rather broad lines with limited resolution. Such spectral characteristics are the result of intrinsic properties of the protein (strain effects, disorder) and the random orientation of molecules in frozen solution. As a consequence, it was already mentioned above for the isotropic contributions of cysteine β-CH_2 protons that some values can only be estimated within a large error margin or cannot be assigned uniquely. In the case of the spin populations for the mixed-valence pair Fe2−Fe3, a range of 1.20 and 1.40 can be given. In this way the coupling of Phe44 Hβ1 still remains inside the line width of the extremal lines along g_1 directions. Combinations of spin populations for Fe2/Fe3 of 1.30/1.30 as well as 1.20/1.40 or 1.40/1.20 can reproduce equally well this coupling and its line behavior. If spin populations on Fe2 and Fe3 of ca. 1.0 are used, the hyperfine splitting would be reduced by more than 2 MHz, requiring however the proton Phe44 Hβ1 to approach the cubane face by 0.4 Å, to a very short distance of 2.9 Å. On the other hand, for spin populations larger than 1.50, an increased distance to the cubane is required for Phe44 Hβ1, but also for other dipolar protons close to the cluster such as Tyr74 Hα, which otherwise would yield discernible larger couplings. Such an expansion of the protein upon going to low temperature is rather improbable.

Concerning the spin populations of the ferric pair, it must be stated that these values have a larger variability than in the case of the mixed-valence pair, as indicated in Chart 1. This is due to the absence of a clearly resolved coupling to a neighboring proton. The information is basically obtained from protons H1, H2, H7, H8, and Hα Cys39, which clearly have a larger variability of parameters than Hβ1 of Phe44. The value of ±0.05 for the spin populations at the cysteinyl sulfur atoms used for simulations implies a maximal dipolar coupling of 0.7 MHz, which is not able to compete with the much larger interaction to the irons or with the isotropic contribution. The simulations also show that a noticeable change of the line behavior of H4 to H6 arises if cysteinyl sulfur atoms spin population values larger than 0.10 are used. However, this would then impair the symmetry of the line variation. Hence, only an upper estimate of <0.10 for the absolute value of the cysteinyl sulfur spin population can be given at present.

Discussion

The hyperfine values of the ^{57}Fe ENDOR interaction are obtained as absolute values because this spectroscopy only yields

transition energies. The group I couplings in Table 1 agree very well with those obtained by Mössbauer spectroscopy for the ferric pair in **1**,[24] **2**,[18] and $[Fe_4S_4(S\text{-}2,4,6\text{-}i\text{-}Pr_3C_6H_2)_4]^{1-}$ (**4**)[53] and are similar to the principal hyperfine couplings obtained by ENDOR for the ferric sites in **2**[52] and in **3**.[22] Furthermore, the group II hyperfine values found by ^{57}Fe ENDOR for **1** (Table 1) are very similar to the values obtained by single-crystal ENDOR in **3**[22] for the mixed-valence pair, albeit they are slightly larger than the values obtained by Mössbauer spectroscopy in **1**[24] and in **4**[53] or by ENDOR in **2**.[52] Comparable hyperfine values have been found in a Q-band ENDOR study of frozen solutions of **2** and HiPIP of *E. halophila* with ^{57}Fe in natural abundance (2.2%).[59] A determination of the sign for these values, in principle achievable by double-ENDOR, was not feasible, probably because of the large experimental line width in comparison to the small bandwidth of the pump frequency and/or insufficient power of the pumping frequency. However, it is obvious that a negative sign should be associated to the values of group II, as these couplings are correlated to the mixed-valence pair.

Only one doublet is observed for the ferric as well as for the mixed-valence pair, indicating that the expected lines of each individual iron ion within a pair overlap, contributing to the observed rather broad resonances. Moreover, a small variation in magnetic parameters, induced for example by a structural disorder of the cubane, together with the powder character, may additionally broaden the lines, preventing a higher spectral resolution basically inherent to ENDOR. A maximal allowed difference of 0.7 MHz in the hyperfine coupling values of the iron ions is estimated from the line width of each doublet, which requires a highly symmetric situation within each pair. Similarly, the two types of ^{57}Fe interactions in **2** showed a comparable small anisotropy and individual contributions of the four irons were not resolvable.[52] For comparison, much larger differences in the extremal hyperfine components of the individual iron ions are obtained from single-crystal measurements of **3**, amounting up to 3.5 and 6 MHz for the ferric and mixed-valence iron ions, respectively.[22]

Additional information on the relative orientation of the *g*- and *A*-tensors can be derived, with some caution, from the variation of the ^{57}Fe resonances across the EPR spectrum. Despite the fact that the lines of the mixed-valence pair are hidden under proton resonances, the minimal coupling has to be roughly associated with the direction of g_1. In the analysis of hyperfine tensors in **3**,[22] both minimal tensor components of the mixed-valence iron ions were found to be nearly parallel to the g_1 direction (with 6° and 25° deviation), but only one of the minimal hyperfine components of the ferric iron ions roughly points along g_1 (26°). In contrast, for **1**, the minimal coupling of the ferric pair is again observed along g_1 (corresponding to the group I resonances, Table 1), suggesting that the minimal components are arranged symmetrically with respect to the *g*-tensor for both the mixed-valence and ferric iron ions. No gross changes of the hyperfine values occur along g_2 and g_3, thus leading to the assumption that rather axial components of the ^{57}Fe tensor are oriented within the g_2,g_3 plane. It is noted that an identical behavior of ^{57}Fe resonances has been observed in **2**.[52] Whether these components for, e.g., the mixed-valence pair are aligned along the bonds between the iron ions and the cubane sulfurs, as was derived from single-crystal model substance, or adopt a different arrangement, cannot be decided on the basis of powder ENDOR measurements.

(59) Houseman, A. L. P.; Oh, B.-H.; Kennedy, M. C.; Fan, C.; Werst, M. M.; Beinert, H.; Markley, J. L.; Hoffman, B. M. *Biochemistry* **1992**, *31*, 2073.

Summing up, the ^{57}Fe-ENDOR results clearly confirm the presence of two distinct iron sites associated to a ferric and a mixed-valence pair. The individual iron ions within each pair seem to be highly symmetric with respect to the metal hyperfine interaction. There is an extensive similarity among proteins and model compounds concerning the magnitude of the ^{57}Fe tensors, further proving the concept that this physical observable constitutes an intrinsic property of the $[Fe_4S_4]^{3+}$ cluster core, regardless of the surrounding environment.

The systematic simulations of proton interactions leave only one possibility for the arrangement of the *g*-tensor with respect to the cluster geometry. The essential findings are that (i) the orientation of the maximal *g*-tensor component g_1 is perpendicular to the cubane face containing the mixed-valence irons and (ii) the directions of g_2 and g_3 are associated to the vectors connecting the ferric and the mixed-valence irons, respectively. They perfectly agree with the configuration found in the single-crystal ENDOR study of **3**, where the deviations between the *g* directions and the same molecular directions were found to be less than 16°.[19,22] Recalling the analysis of the dipolar interactions, spin populations around +1.30 on each mixed-valence iron are required (see Chart 1). This value is comparable to the values of 1.36 and 1.29 for the two mixed-valence irons derived from the dipolar tensors of protons in **3**. The spin values of the ferric pair (ca. −0.70), determined with lower precision, are also similar to the values of −0.62 and −0.72 found in **3**.[23] As pointed out by Mouesca et al.,[23] these experimental spin densities or spin populations, with or without corrections to account for spin relocalization from the sulfur atoms, can be related to vector-coupling coefficients K_i theoretically derived for the $|^9/_2,4,^1/_2\rangle$ spin state as $K(\mathrm{mv}) = +1.83$, $K(\mathrm{f}) = -1.33$ and for the $|^7/_2,3,^1/_2\rangle$ spin state as $K(\mathrm{mv}) = +1.50$, $K(\mathrm{f}) = -1.00$.[39] From the comparison it seems that the experimental spin populations of +1.3 and −0.7 correlate more closely to the coefficients K_i of the $|^7/_2,3,^1/_2\rangle$ state.[23] The isotropic ^{57}Fe hyperfine coupling found in **1** by Mössbauer and ENDOR spectroscopy (Table 1) are also fairly close to the values of −33.0 MHz for the mixed-valence and +20.0 MHz for the ferric irons predicted by theoretical considerations for the $|^7/_2,3,^1/_2\rangle$ state[23] as compared to values of −38.5 and +26.7 MHz for respective irons expected in a $|^9/_2,4,^1/_2\rangle$ spin state.[16,39] Recently, it has been shown that an admixture of ground states $|^9/_2,4,^1/_2\rangle$ and $|^7/_2,4,^1/_2\rangle$, with a larger contribution of the former, is reproducing Mössbauer, EPR, and NMR data better than any proposed pure $|S_{34},S_{12},S\rangle$ state.[40] For instance, a ground-state function given by $(0.81)^{1/2}|^9/_2,4,^1/_2\rangle - (0.19)^{1/2}|^7/_2,4,^1/_2\rangle$ yields coupling coefficients values of +1.26 and −0.76 close to the spin populations given in Chart 1 for the mixed-valence and ferric pair, respectively. However, a clear distinction of the models does not seem feasible due to the variability of spin populations, particularly of the ferric irons, and to the indeterminate relocalizable sulfur spin population.

Let us now turn to the interpretation of the two sets of isotropic contributions to the ENDOR spectrum of the eight cysteine protons, presented in Table 2. The main difference between set I and set II refers to protons H3−H6, which are close to the mixed-valence iron ions. The isotropic values for some of the cysteine protons that could be directly determined from simulations are marked with an asterisk in Table 2, while the values in parentheses represent estimates. For the sake of completeness also the estimated values are included in the analysis below, but their lower significance should be kept in mind. For both sets, the protons of cysteines bound to the mixed-valence iron ions require positive isotropic couplings, while those at ferric iron ions require negative values. To discriminate

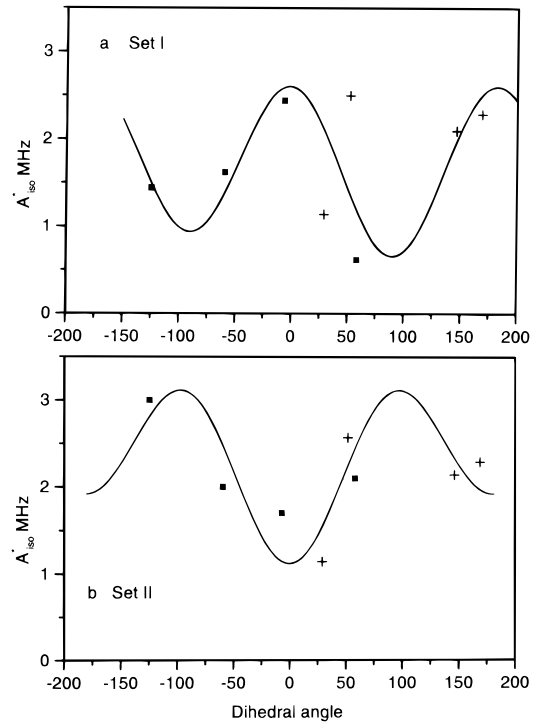

Figure 6. Plot of the normalized isotropic couplings of cysteine β-CH_2 protons (set I in a, set II in b) versus their dihedral angles of the MD structure. The protons close to the ferric irons are represented by crosses, and those close to the mixed-valence irons are marked as filled squares. (For coupling values of both sets see Table 2). The curves were calculated with the empirical formula (eq 1). Details are described in the text.

between set I and set II, the simulated values are rescaled to a spin population of 1 at each iron. The coupling should then depend mainly on the geometry of the cysteine arrangement.[23,60] An empirical formula has been found that relates the Fe−S−C−H dihedral angle of each cysteine β-CH_2 proton from the MD structure to its isotropic hyperfine coupling as given below[14,60]

$$A^*_{iso}(\theta) = A \sin^2(\theta) + B \cos(\theta) + C \qquad (1)$$

in which $A^*_{iso}(\theta)$ indicates the rescaled isotropic hyperfine values.[61] The data for both set I and set II are compared in Figure 6a,b. The curves were calculated from the fit of eq 1 starting with the coefficients derived from ENDOR data of **3**[23,62] (A = 1.52, B = −0.07, C = 1.21). For set II the parameters A = 1.57, B = −0.4, and C = 1.52 obtained are closely related to these values. For the fit of set I (Figure 6a) a phase shift of ca. 90° had to be introduced as the major difference. The comparison indicates that set II is the only one consistent with the expected angular dependence and is thus considered to represent the good isotropic coupling constants.

E. halophila iso-II HiPIP has been extensively studied by NMR spectroscopy in its reduced and its paramagnetic oxidized state.[14,27,28] The study of the connectivities and the temperature dependence of the large positive and negative contact hyperfine shifted resonances (up to 98 and −32 ppm, respectively, Table 2) observed in the ^{1}H NMR spectra of **1** has allowed their assignment to the β-CH_2 protons of the cysteine residues close to the mixed-valence and ferric iron ions of the $[Fe_4S_4]^{3+}$ cluster in **1**. Thus, a correlation of the isotropic couplings obtained from NMR and ENDOR spectroscopies can be attempted. The shifts of protons coupled to an electron by hyperfine interaction are related to the Fermi contact term A by eq 2,[14,63] in which the

$$\delta_j^{con} = \frac{2\pi g \mu_B}{3 g_N k T} \frac{A_j}{h} \sum_i C_{ji} S_i'(S_i'+1) \frac{(S_i'+1)\exp(-E_i/kT)}{\sum_i (2S_i'+1)\exp(-E_i/kT)} \qquad (2)$$

S_i' values are the total spin of the cluster for each ith level, at energy E_i, of the coupled system ($S_1' = {}^1/_2$ for the ground state), and all other constants have their usual physical meaning. The C_{ji} values are given by eq 3,[14] where i refers to the energy level

$$C_{ji} = \frac{\langle S_{jz} \rangle_i}{\langle S_z' \rangle_i} \qquad (3)$$

and j to the particular metal ion to which the cysteine bearing the proton is bound. In our model, $C_{1i} = C_{2i}$ refer to the ferric iron ions and $C_{3i} = C_{4i}$ refer to the mixed-valence iron ions. The A_{iso} values from ENDOR are given by A_jC_{j1}, i.e., by the product of the hyperfine coupling constant in the absence of magnetic interactions between the iron ions (A_j) multiplied by the C_{j1} coefficient of the ground state which is the only relevant state in the low-temperature ENDOR experiment. Calculation of δ_j^{con} values from eq 2 would require knowledge of the E_i values for all the levels populated at the temperature of the NMR experiment and their relative spin eigenfunction (or admixtures thereof). However, the two groups of protons from the ferric and the mixed-valence pairs should sense the same S_i' spin ladder, and thus their shifts should depend only on their individual A_j values and on either of the two sets of C_{ji} coefficients. Therefore, the hyperfine shifts should be convertible directly to hyperfine values, provided two different factors are used for the two groups of protons. For normalization, in each of the groups, the most reliable A_{iso} value from ENDOR was used (i.e., H5 for the first group and H7 for the second). By applying the factors 3.9/98 and 1.0/21 MHz/ppm, respectively, thus derived, we find the calculated A_{iso} values for the other protons shown in Table 2 in good agreement with the values experimentally derived from ENDOR, with the exception of H4 which is, however, one of the least reliable ENDOR values (Table 2).

It should be noted that the ratio of the conversion factors (0.84) reflects the effect of the population of excited S_i' states. This ratio should be unity if the NMR experiments could be performed at 4 K and is expected to approach zero and tend to −1 at infinite temperature. A value of 0.84 evidences the substantial separation of the ground state from the first excited states in oxidized HiPIPs, in turn confirming that the magnetic coupling J constants are in the hundreds of wavenumbers range.

The last column in Table 2 gives the isotropic couplings derived from the detailed proton ENDOR single-crystal study of the oxidized $[Fe_4S_4]$ center in the model compound (**3**). All eight thiolate-CH_2 protons are listed, but a comparison with the present ENDOR results is warranted only for the protons marked in column 2, which are, with the exception of H7, the protons

(60) Bertini, I.; Capozzi, F.; Luchinat, C.; Piccioli, M.; Vila, A. J. *J. Am. Chem. Soc.* **1994**, *115*, 651.

(61) The formula used by Lamotte et al.[23] is algebraically equivalent to eq 1, although the coefficients have different physical meanings.

(62) Noodleman, L; Chen, J.-L.; Case, D. A.; Giori, C.; Rius, G.; Mouesca, J.-M.; Lamotte, B. *Nuclear Magnetic Resonance of Paramagnetic Macromolecules*; Kluwer Academic Publishers: Dordrecht, The Netherlands, 1995; pp 339−367.

(63) Bertini, I.; Luchinat C. NMR of Paramagnetic Substances. *Coord. Chem. Rev.* **1996**, *150*, 1−296.

Table 3. Principal Dipolar Tensor Components of Cysteine β-CH_2 Protons Close to Mixed-Valence Irons from **1** and of Thiolate-CH_2 Protons of **3** for Comparison

proton (Chart 1)	principal values of A_{dip} (MHz)	principal directions with respect to the *g*-tensor frame[a]			principal values A_{dip} (MHz) of ref 23[b]
H5 (Cys55 Hβ2)	3.216	−0.261	−0.194	0.946	4.26
	−1.711	0.930	−0.323	0.176	−2.26
	−1.589	−1.589	−0.922	−0.262	−2.00
H6 (Cys55 Hβ1)	−3.568	0.894	−0.426	−0.135	8.71
	−2.930	0.434	0.673	0.598	−6.27
	6.323	−0.173	−0.595	0.785	−2.44
H3 (Cys42 Hβ2)	7.010	−0.364	−0.783	−0.504	3.35
	−4.162	−0.869	0.475	−0.141	−1.95
	−2.978	−0.367	−0.385	0.847	−1.40
H4 (Cys42 Hβ1)	−4.043	0.913	−0.261	0.314	7.00
	−3.073	−0.418	−0.728	0.544	−4.95
	6.910	0.092	−0.630	−0.771	−2.05

[a] The principal directions are related only to the cysteine β-CH_2 protons of the protein. [b] The values were related to protein protons in the same way as in Table 2.

of the mixed-valence iron bound cysteines. One should not expect to be able to generate a direct correlation between the model compound and the protein. For one thing, the model compound displays in EPR six oxidized species with somewhat different *g*-tensor values produced by irradiation at low temperatures[21] and ENDOR data are available only for one of them. Furthermore, the sequence-specific proton assignment which is available for the protein cannot be transferred to the model compound. Nevertheless, a comparison of results should yield a general impression of the interrelation of data. For this we have grouped the mixed-valence bound thiolate-CH_2 protons of **3** such as to associate the largest isotropic coupling with the largest value of the protein. Then the magnitude of values, in general, agrees well with those of protein **1** as well as with the results of the NMR study.[27] In fact, the tendency of couplings to be different for the protons of the same thiolate-CH_2 in the model compound due to the different dihedral angles is reflected in the protein (cf., e.g., H5 and H6 in the protein nomenclature) as is the trend that the couplings of the CH_2 protons of the two thiolate groups which are connected to the two mixed-valence iron ions have different values.

Another relation between the ENDOR data of the model compound **3** and the protein concerns the dipolar parts of the proton interaction tensors. Table 3 lists the respective values. Again, only the four cysteines of the mixed-valence pair are considered since the other protons in the protein are much less well determined. Keeping in mind the same reservation concerning the proton assignment in **3** and in the protein discussed above as well as the error margins of the simulations for the protein, there is a relatively fair agreement, if not for the numerical values then for the tendencies of couplings. Consider the values for the two cysteine protons H5 and H6 which could be related to the interactions A6 and A5 in the model compounds according to their isotropic couplings as discussed above. As in the model compound, the proton with the larger isotropic part (H5) has the smaller dipolar tensor whereas the one with the smaller isotropic coupling has a larger dipolar contribution. This trend, however, cannot be followed through for interactions H3 and H4 since the distinction between the isotropic parts in the protein is much less distinct. Also, the differences between dipolar parts for these protons are smaller than they are in the model compound. Altogether, this comparison shows a reasonable agreement between model compound and protein and supports the conclusions about the validity of the point-dipolar model calculations of dipolar interactions discussed in detail for the model compound results.[23] One should note that the dipolar parts in the model compounds are more rhombic in symmetry than are the respective protein tensors. Taken together with the slightly enhanced absolute values in the model one might conclude that the distances of the respective protons to the spin centers are shorter than they are in the protein.

A final remark concerns the structure of the cluster which was derived from a molecular dynamics approach. For ENDOR simulations only small changes in hydrogen positions (within ± 0.05 Å) were introduced to improve the match with experimental frequency positions. This refers not only to the directly ligating cysteines but also to amino acid residues in the immediate environment of the cluster, in particular Phe44 and Tyr74. Due to the high sensitivity of dipolar couplings in ENDOR on the distance it is concluded that the MD structure is a good model of the structure of **1** (in accordance with NMR results[27]) and that no gross changes in the cluster geometry are occurring upon freezing the protein.

Conclusions

The work described in this report represents, to our knowledge, the first combined ^{57}Fe- and ^{1}H-ENDOR analysis of electronic and structural details of a $[Fe_4S_4]^{3+}$ cluster of a high-potential iron−sulfur protein in frozen solution. Two distinct iron sites associated with a ferric and a mixed-valence pair were discerned from ^{57}Fe ENDOR, exhibiting a high degree of internal symmetry. The iron hyperfine interactions determined agree well with data obtained from Mössbauer experiments on *E. halophila* iso-II HiPIP and related proteins as well as with ENDOR results on model systems, favoring a $|^{7}/_{2},3,^{1}/_{2}\rangle$ state or an admixture of $|^{9}/_{2},4,^{1}/_{2}\rangle$ and $|^{7}/_{2},4,^{1}/_{2}\rangle$ states as the ground state. The analysis of dipolar contributions to proton hyperfine interaction allowed determination of the orientation of the *g*-tensor with respect to the molecular frame, identification of the mixed-valence and ferric irons with specific iron sites of the proposed structure, and derivation of the spin population within the cluster. These results independently support the assignments obtained by NMR of proteins in solution and ENDOR on single crystals of model substances. Moreover, they confirm the concept of the spin vector coupling model and theoretical considerations derived on its basis, thus providing a link to the analysis of electronic states based on NMR results obtained at room temperature.

Acknowledgment. This work was funded by a grant from the Deutsche Forschungsgemeinschaft within the priority program "Bioinorganic Chemistry".

JA980442Z